

JET ENERGY AND OTHER PARAMETERS FOR THE AFTERGLOWS OF GAMMA-RAY BURSTS
980703, 990123, 990510, AND 991216 DETERMINED FROM MODELING OF MULTI-FREQUENCY DATA

A. PANAITESCU

Dept. of Astrophysical Sciences, Princeton University, Princeton, NJ 08544

AND

P. KUMAR

Institute for Advanced Study, Olden Lane, Princeton, NJ 08540

ABSTRACT

We model the radio, optical, and X -ray emission for the afterglows of GRB 980703, 990123, 990510, and 991216, within the framework of relativistic jets, to determine their physical parameters. The models that yield acceptable fits to the data have jet energies mostly between 10^{50} to 10^{51} erg and initial opening angles between 1° and 4° . The external medium density is uncertain by at least one order of magnitude in each case, being around 10^{-3} cm^{-3} for GRB 980703 and 990123, $\sim 10^{-1} \text{ cm}^{-3}$ for GRB 990510, and $\sim 3 \text{ cm}^{-3}$ for GRB 991216. If the jets are uniform (i.e. there are no angular gradients of the energy per solid angle) then the 20 keV – 1 MeV radiative efficiency during the GRB phase must have been at least 2-3% for GRB 990510, 20% for GRB 990123, and 30% for GRB 991216.

Subject headings: gamma-rays: bursts - ISM: jets and outflows - methods: numerical - radiation mechanisms: non-thermal - shock waves

1. INTRODUCTION

There are two basic quantities one needs to try understanding the nature of any astronomical source – the distance and the energy of the source. For the long duration GRBs, lasting more than 10 seconds, the former is well established to be cosmological. However, the energy associated with the GRBs remains uncertain.

The efficiency of producing γ -ray emission in the generally accepted internal shock model (Mészáros & Rees 1994), which can explain the observed temporal variability, is less than a few percent (Kumar 1999, Lazzati, Ghisellini & Celotti 1999, Panaitescu, Spada & Mészáros 1999, see also Beloborodov 2000). This suggests that the total energy in the explosion is larger than the energy observed in γ -rays by a factor of 20–50.

The goal of this work is to infer the physical parameters of the ejecta, including their energy and the external medium density, from modeling of radio, optical and X -ray data for GRB afterglows with known redshifts. The modeling is carried out in the framework of collimated ejecta interacting with an isotropic external medium. The model is described in §2 and the results of the numerical calculations for individual afterglows are given in §4.

2. DESCRIPTION OF THE MODEL

In calculating the jet dynamics, we assume that the energy and baryon density within the ejecta do not have an angular dependence, and that the external medium is isotropic. We also assume that, at any time, the physical parameters and bulk Lorentz factor Γ are the same in the entire swept up external gas. We include the effect of radiative energy losses on the jet dynamics.

For the calculation of synchrotron emission, we assume a tangled magnetic field and that the electrons accelerated at shock have a power-law distribution. The electron distribution resulting from the continuous injection at shock and adiabatic+radiative cooling is approximated by broken power-law, with a break at the minimum random Lorentz factor of the

freshly injected electrons and another one at the cooling electron Lorentz factor. In calculating the received flux, the swept up gas is approximated as a surface, i.e. the thickness of the emitting shell is ignored. The effect of this surface curvature on the photon arrival time and energy is taken into account.

2.1. Dynamics

The interaction between the relativistic ejecta that generated the GRB with the external gas continuously decelerates the jet and heats the newly swept up gas. Assuming that the heated gas has a uniform temperature, equal to that of the freshly shocked fluid, the total energy of the GRB remnant is:

$$E(r) = m(r)(\Gamma^2 - 1) + m_0(\Gamma - 1), \quad (1)$$

where m_0 is the mass of the ejecta, whose Lorentz factor and energy at the end of the GRB phase are Γ_0 and $E_0 = (\Gamma_0 - 1)m_0c^2$, respectively.

In the above equation, m is the mass of the swept up external gas, given by

$$dm(r) = \Omega(r)\rho(r)r^2 dr, \quad (2)$$

where $\rho(r) \propto r^{-s}$ is the external medium density ($s = 0$ for homogeneous gas, $s = 2$ for a wind ejected at constant speed before the release of the ultra-relativistic ejecta), and $\Omega(r)$ is solid angle of the jet.

The jet half opening angle increases due to the lateral spreading of the jet at the local sound speed c_s :

$$r d\theta = c_s dt' = \Gamma^{-1} c_s dt_{lab}, \quad (3)$$

t' and t_{lab} being the time measured in the ejecta comoving and laboratory frames, respectively. The speed of sound is (see Huang et al. 2000)

$$c_s^2 = \frac{\hat{\gamma}(\hat{\gamma} - 1)u'}{\rho' + \hat{\gamma}u'} c^2 = \frac{\hat{\gamma}(\hat{\gamma} - 1)(\Gamma - 1)}{1 + \hat{\gamma}(\Gamma - 1)} c^2, \quad (4)$$

where $u' = (\Gamma - 1)\rho'$ and ρ' are the comoving internal energy and rest mass densities, respectively, and $\hat{\gamma}$ is the adiabatic index. In the relativistic limit $\hat{\gamma} = 4/3$ and $c_s = c/\sqrt{3}$, while for

non-relativistic speeds $\hat{\gamma} = 5/3$ and $c_s = (\sqrt{5}/3)v$, where v is the radial expansion speed. We relate the adiabatic index with Γ through a simple formula, which has the above asymptotic limits.

The energy losses through synchrotron and inverse Compton emissions is given by

$$\frac{dE}{dt_{lab}} = -\frac{\sigma_e c}{6\pi} \frac{m(r)}{m_p} B^2 (Y+1) \int_{\gamma_m}^{\gamma_M} \gamma^2 d\mathcal{N}(\gamma), \quad (5)$$

where B is the magnetic field intensity, Y the Compton parameter, \mathcal{N} is the normalized electron distribution (§2.2), and γ is the electron random Lorentz factor.

Equations (1), (2), (3) and (5) are solved numerically, subject to the boundary conditions: $\Gamma(0) = \Gamma_0$, $m(0) = 0$, $\theta(0) = \theta_0$, and $E(0) = E_0$.

2.2. Electron Distribution and Spectral Breaks

The magnetic field intensity is parameterized relative to its equipartition value

$$B^2 = 8\pi \rho' c^2 (\Gamma - 1) \varepsilon_B = 32\pi \varepsilon_B \rho(r) c^2 (\Gamma - 1) \frac{\hat{\gamma}\Gamma + 1}{\hat{\gamma} - 1}, \quad (6)$$

where ρ' is the comoving frame rest-mass density.

The distribution of the electrons accelerated by the forward shock and injected in down-stream is assumed to be a power-law of index p

$$\mathcal{N}_i(\gamma) \propto \gamma^{-p}, \quad \gamma_i < \gamma < \gamma_M, \quad (7)$$

where γ_i is the minimum, injected electron Lorentz factor, parameterized relative to its value at equipartition,

$$\gamma_i = \varepsilon_e \frac{m_p}{m_e} (\Gamma - 1), \quad (8)$$

and γ_M is an upper limit, determined by the conditions that the acceleration timescale of such electrons does not exceed the radiative losses timescale, and that the total energy in the injected electrons does not exceed a certain fraction ϵ of the available internal energy. The former condition leads to

$$\gamma_M^{(1)} = \left[\frac{3e}{n_g \sigma_e} \frac{1}{B(Y+1)} \right]^{1/2}, \quad (9)$$

where n_g is the ratio of the acceleration timescale to the gyration time. The latter condition can be written as

$$m_e \int_{\gamma_i}^{\gamma_M^{(2)}} \gamma d\mathcal{N}_i(\gamma) = \epsilon m_p (\Gamma - 1), \quad (10)$$

where \mathcal{N}_i is normalized (to unity), and m_e and m_p are the electron and proton mass, respectively. Equation (10) leads to an algebraic equation which can be solved numerically. The upper limit γ_M is the minimum between $\gamma_M^{(1)}$ and $\gamma_M^{(2)}$ above. Unless n_g is larger than about 10^3 , the upper limit given in equation (9) is sufficiently high that the synchrotron emission from $\gamma_M^{(1)}$ -electrons is above the soft X-ray domain. However if $p \lesssim 2.5$ and ϵ is not much larger than ε_e , the upper limit given by equation (10) may be sufficiently low to yield a break of the afterglow emission at the frequencies of interest (X-rays and even optical). For numerics we shall use $n_g = 10$ and $\epsilon = 0.5$,

the latter corresponding to equipartition between electron and protons.

The distribution of cooled electrons is a power-law of index 2 if the electrons are cooling faster than the dynamical timescale, and a power-law steeper by unity than the injected distribution in the opposite case (Sari, Piran & Narayan 1998). Therefore the electron cooling distribution resulting from injection at shock and radiative cooling is

$$\mathcal{N}(\gamma) \propto \begin{cases} \gamma^{-2} & \gamma_c < \gamma < \gamma_i \\ \gamma^{-(p+1)} & \gamma_i < \gamma < \gamma_M \end{cases}, \quad (11)$$

for fast cooling electrons ($\gamma_c < \gamma_i$), and

$$\mathcal{N}(\gamma) \propto \begin{cases} \gamma^{-p} & \gamma_i < \gamma < \gamma_c \\ \gamma^{-(p+1)} & \gamma_c < \gamma < \gamma_M \end{cases}, \quad (12)$$

for slow cooling electrons ($\gamma_i < \gamma_c$). In equations (11) and (12), γ_c is the cooling electron Lorentz factor, defined by the equality of its radiative cooling timescale with the dynamical timescale:

$$\gamma_c = 6\pi \frac{m_e c}{\sigma_e} \frac{1}{t' B^2 (Y+1)}. \quad (13)$$

The Compton parameter Y is given by

$$Y = \frac{4}{3} \tau_e \int_{\gamma_m}^{\gamma_M} \gamma^2 d\mathcal{N}(\gamma), \quad (14)$$

where $\gamma_m = \min(\gamma_i, \gamma_c)$ and τ_e is the optical thickness to electron scattering:

$$\tau_e = \frac{\sigma_e}{m_p} \frac{m(r)}{\Omega(r)r^2}. \quad (15)$$

The Klein-Nishina effect reduces the inverse Compton losses above an electron Lorentz factor γ_{KN} approximated as the geometric mean of *i*) the electron Lorentz factor for which scattering of the synchrotron photons emitted by such an electron occurs at the Klein-Nishina limit and of *ii*) the electron Lorentz factor for which scattering of the synchrotron photons emitted by γ_m -electrons is at the same limit. The comoving frame synchrotron characteristic frequency for an electron of Lorentz factor γ is

$$\nu'(\gamma) = \frac{3}{16} \frac{e}{m_e c} B \gamma^2. \quad (16)$$

We take into account the Klein-Nishina reduction by calculating the integral in equation (14) up to γ_{KN} if $\gamma_{KN} < \gamma_M$, and by switching off the inverse Compton losses above γ_{KN} in the integral given in equation (5).

The synchrotron self-absorption frequency in the fluid rest frame is at $\nu'_a = \nu'(\gamma_a)$ with γ_a given by (see Panaitescu & Kumar 2000)

$$\gamma_a = \left(\frac{5e}{\sigma_e} \frac{\tau_e}{B} \right)^{3/10} \gamma_m^{-1/2}. \quad (17)$$

This equation is valid only if $\gamma_a < \gamma_m$.

2.3. Received Flux

The synchrotron spectrum is approximated as piece-wise power-law (see Sari et al. 1998) with breaks at the injection, cooling, and absorption breaks given by equations (16), (8), (13), and (17).

To calculate the afterglow flux seen by the observer, we consider that the emitting shell is infinitely thin and that the observer is located on the jet axis. Consider an annular region of area $\delta A = 2\pi r^2 \delta\mu$, with $\mu = \cos\omega$, where ω is the polar angle, measured relative to the jet axis. The energy emitted in the comoving frame per unit time and frequency is $\delta L'_{\nu'} = P'_{\nu'} \Sigma_e \delta A$, where $P'_{\nu'}$ is the radiative comoving power per electron and Σ_e is the electron surface density. The infinitesimal comoving energy emitted per solid angle $(1/4\pi)\delta L'_{\nu'} d\nu' dt'$ is relativistically beamed toward the observer by a factor \mathcal{D}^2 and boosted in frequency by a factor \mathcal{D} , where $\mathcal{D} = [\Gamma(1 - \beta\mu)]^{-1}$, with $\beta = v/c$. Therefore the infinitesimal flux dF_ν received by the observer at frequency $\nu = \mathcal{D}\nu'$, during $\Delta t = c^{-1}r\delta\mu$ satisfies

$$dF_\nu d\nu \delta t = \frac{1+z}{4\pi d_L^2} \mathcal{D}^3 P'_{\nu'} \Sigma_e dt' d\nu' \delta A, \quad (18)$$

where $P'_{\nu'}$ is the sum of synchrotron and inverse Compton emissions, z is the afterglow redshift, and d_L is the luminosity distance. We assume a Universe with $H_0 = 65 \text{ km s}^{-1} \text{ Mpc}^{-1}$, $q_0 = 0.1$, and $\Lambda = 0$.

The flux received by the observer at time t is that given by equation (18), integrated over the entire evolution of the source. Using $dt' = dt_{lab}/\Gamma = dr/(\beta c\Gamma)$ and relating the electron surface density to the jet mass and area, $\Sigma_e = m(r)/(m_p \Omega r^2)$, equation (18) leads to

$$F_\nu(t) = \frac{1+z}{2m_p d_L^2} \int \frac{dr}{\beta \Gamma^3 (1 - \beta\mu)^2} \frac{P'_{\nu'}(r)m(r)}{r\Omega(r)}, \quad (19)$$

with μ given by the condition that light emitted from location (r, μ) arrives at observer at time $t = t_{lab} - (r/c)\mu$. Thus equation (19) takes into account the spread in the photon arrival time due to the spherical curvature of the jet surface. In all our calculations it is assumed that the observer is on the jet axis.

3. ANALYTICAL CONSIDERATIONS

So far there are five afterglows (990123, 990510, 991216, 000301c, 000926) for which a break in the optical emission has been identified. In all these cases the break is seen at or after $t = 1$ day. Within the framework of uniform ejecta interacting with isotropic media, there are two possible causes for such a break: the passage of a break frequency (injection, ν_i , cooling, ν_c , or that due the upper cut-off of the electron distribution, ν_M), or the edge of the jet becoming visible to the observer (plus the changing dynamics due to the lateral spreading of the jet).

One can show that, within a factor of order unity, the break frequency ν_i is the same for both types of external medium:

$$\nu_i \sim 10^{13} (z+1)^{1/2} \mathcal{E}_{0.54}^{1/2} \varepsilon_e^2 \varepsilon_{B,-1}^{1/2} t_d^{-3/2} \text{ Hz}, \quad (20)$$

where $\mathcal{E}_0 = 4\pi(E_0/\Omega_0)$ is the jet isotropic equivalent energy, t_d is observer time in days, and the usual notation $A_n = 10^{-n} A$ was used. Equation (20) shows that, unless the isotropic equivalent energy exceeds 10^{56} erg and the magnetic field is close to equipartition (ε_e cannot be much higher than 0.1, as the fractional energy in electrons must be below unity), ν_i is below the

optical range at $t \gtrsim 1$ day. Therefore it is very unlikely that the optical light-curve breaks are due to the passage of ν_i through the observational band. Moreover, if this were the case, then, at times before the light-curve break, the temporal index α of the light-curve decay, $F_\nu(t) \propto t^{-\alpha}$, would be at most 1/4, which is much smaller than the observed α 's.

3.1. Passage of the Cooling Break

We consider here the afterglow emission at early times, when the effects due to collimation of ejecta are negligible, but sufficiently large that $\nu_i < \nu$. In this case, the afterglow light-curves for slow cooling electrons ($\nu_i < \nu_c$) are given by (see Panaitescu & Kumar 2000)

$$F_{\nu > \nu_i} \propto \begin{cases} t^{-(3p-3)/4} & \nu < \nu_c \\ t^{-(3p-2)/4} & \nu_c < \nu, Y < 1 \\ t^{-(3p/4)+1/(4-p)} & \nu_c < \nu, Y > 1, 2 < p < 3 \\ t^{-(3p/4)+1} & \nu_c < \nu, Y > 1, 3 < p \end{cases} \quad (21)$$

for a homogeneous external medium ($s = 0$), where the last two rows represent the case when the electron cooling is dominated by inverse Compton scatterings. For a wind-like medium ($s = 2$) and slow cooling electrons

$$F_{\nu > \nu_i} \propto \begin{cases} t^{-(3p-1)/4} & \nu < \nu_c \\ t^{-(3p-2)/4} & \nu_c < \nu, Y < 1 \\ t^{-(3p/4)+p/(8-2p)} & \nu_c < \nu, Y > 1, 2 < p < 3 \\ t^{-(3p/4)+3/2} & \nu_c < \nu, Y > 1, 3 < p \end{cases} \quad (22)$$

The second row of equations (21) and (22) also gives the light-curve for $\nu_i < \nu$ and fast cooling electrons.

The temporal evolution of the cooling break frequency ν_c for $s = 0$ and slow cooling electrons is given by

$$\nu_c \propto \begin{cases} t^{-1/2} & Y < 1 \\ t^{-(8-3p)/(8-2p)} & Y > 1, 2 < p < 3 \\ t^{1/2} & Y > 1, 3 < p \end{cases} \quad (23)$$

For $s = 2$ and slow cooling electrons

$$\nu_c \propto \begin{cases} t^{1/2} & Y < 1 \\ t^{(3p-4)/(8-2p)} & Y > 1, 2 < p < 3 \\ t^{5/2} & Y > 1, 3 < p \end{cases} \quad (24)$$

The first row also gives the evolution of ν_c for fast cooling electrons, in which case Y is time-independent.

For a homogeneous medium, equation (23) shows that ν_c increases in time if the electron cooling is dominated by inverse Compton and if $p > 8/3$. From equation (21), the passage of ν_c through the observational band changes the light-curve decay index by

$$(\Delta\alpha)_c = \begin{cases} 1/4 & Y < 1 \\ (8-3p)/(16-4p) & Y > 1, 2 < p < 8/3 \\ (3p-8)/(16-4p) & Y > 1, 8/3 < p < 3 \\ 1/4 & Y > 1, 3 < p \end{cases} \quad (25)$$

Note $(\Delta\alpha)_c > 0$, i.e. the passage of ν_c always steepens the light-curve decay, even if ν_c increases in time, and that $(\Delta\alpha)_c < 1/4$. In the case where ν_c is above optical and below X-ray, the temporal indices of the X-ray and optical light-curves differ by $\alpha_x - \alpha_o = (\Delta\alpha)_c > 0$ if ν_c decreases in time,

and by $\alpha_x - \alpha_o = -(\Delta\alpha)_c < 0$ if ν_c increases in time. Thus, for $s = 0$, the X -ray emission decays faster than the optical one if $Y < 1$ or $Y > 1$ and $p < 8/3$.

For a wind-like medium equation (24) shows that ν_c always increases in time. From equation (22), the passage of ν_c yields

$$(\Delta\alpha)_c = \begin{cases} 1/4 & Y < 1 \\ (3p-4)/(16-4p) & Y > 1, 2 < p < 3 \\ 5/4 & Y > 1, 3 < p \end{cases} \quad (26)$$

Note that $1/4 < (\Delta\alpha)_c < 5/4$. For $\nu_o < \nu_c < \nu_x$, the X -ray and optical indices differ by $\alpha_x - \alpha_o = -(\Delta\alpha)_c < 0$. Hence, for $s = 2$, the X -ray emission always decays slower than the optical one.

3.2. Collimation of Ejecta

If the ejecta is collimated, the decay of the afterglow emission steepens around the time t_j when $\Gamma\theta = 1$, due to the altered jet dynamics and that the observer sees the edge of the jet. For $s = 0$

$$t_j = 1.2 (z + 1) (\mathcal{E}_{0.54} \theta_{0,-1}^8 n_0^{-1})^{1/3} \text{ day} \quad (27)$$

The coefficient above was determined numerically from the arrival time of the photons moving toward the observer along the jet axis. Photons emitted from other regions on the jet surface arrive later by a factor up to ~ 4 .

Around t_j the jet dynamics changes from a quasi-spherical expansion with $\Gamma \propto r^{-3/2} \propto t^{-3/8}$ for $s = 0$ ($\Gamma \propto r^{-1/2} \propto t^{-1/4}$ for $s = 2$) to a sideways expansion characterized by $\Gamma \propto e^{-kr} \propto t^{-1/2}$ (Rhoads 1999). During the lateral spreading phase ($t > t_j$) the cooling frequency evolution is

$$\nu_c \propto \begin{cases} t^0 & Y < 1 \\ t^{2(p-2)/(4-p)} & Y > 1, 2 < p < 3 \\ t^2 & Y > 1, 3 < p \end{cases} \quad (28)$$

assuming slow cooling electrons ($\nu_i < \nu_c$). Then it can be shown that, at $t > t_j$, the light-curve is given by

$$F_{\nu > \nu_i} \propto \begin{cases} t^{-p} & \text{any } \nu, Y < 1 \\ t^{-p+(p-2)/(4-p)} & \nu_c < \nu, Y > 1, 2 < p < 3 \\ t^{-(p-1)} & \nu_c < \nu, Y > 1, 3 < p \end{cases} \quad (29)$$

Evidently, as the source slows down, the Y parameter eventually falls below unity and the last two cases given in equation (29) approach asymptotically $F_\nu \propto t^{-p}$. The results given in equations (28) and (29) ignore multiplying terms that are powers of the jet radius r , which increases logarithmically with the observer time. With the same approximation, they also hold for a jet interacting with a pre-ejected wind. Furthermore, these results are accurate only at times when the afterglow is very relativistic. From numerical calculations we found that, for the first case given in equation (29), the decay index α is approximated by p with an error less than 10% if $\Gamma \gtrsim 10$.

Using equations (21), (22), and (29) it can be shown that, for $\nu > \nu_i$, the magnitude of the break due to collimation of ejecta is

$$(\Delta\alpha)_j = \begin{cases} (p+3)/4 & \nu < \nu_c \\ (p+2)/4 & \nu_c < \nu, Y < 1 \\ p/4 + 1/(4-p) & \nu_c < \nu, Y > 1, 2 < p < 3 \\ (p+4)/4 & \nu_c < \nu, Y > 1, 3 < p \end{cases} \quad (30)$$

for $s = 0$ and

$$(\Delta\alpha)_j = \begin{cases} (p+1)/4 & \nu < \nu_c \\ (p+2)/4 & \nu_c < \nu, Y < 1 \\ p/4 + p/(8-2p) & \nu_c < \nu, Y > 1, 2 < p < 3 \\ (p+6)/4 & \nu_c < \nu, Y > 1, 3 < p \end{cases} \quad (31)$$

for $s = 2$. The finite opening of the ejecta yields $\Delta\alpha = 3/4$ for $s = 0$ and $\Delta\alpha = 1/2$ for $s = 2$ (Panaitescu, Mészáros & Rees 1998) when the jet edge becomes visible, the remainder of the steepening being due to the sideways expansion of the jet (Kumar & Panaitescu 2000). Equations (30) and (31) show that, if $p > 2$, $(\Delta\alpha)_j > 1$ for $s = 0$ and $(\Delta\alpha)_j > 3/4$ for $s = 2$.

3.3. What Can We Infer from the X -ray and Optical Decay Indices ?

The most important difference between a break due to passage of ν_c and one due to collimation of ejecta is the chromaticity of the former and the achromaticity of the latter. This would be the best criterion to distinguish between them if optical and X -ray observations spanning the same 1–2 decades in time, around the time when the break is seen, are available.

The analytical results presented in §3.1 and §3.2 allow us to draw some conclusions even when the existence of simultaneous X -ray and optical light-curve breaks cannot be clearly established. Equations (25), (26), (30), and (31) show that optical break magnitudes $\Delta\alpha < 3/4$ can be produced *only* by the passage of the cooling break, while $\Delta\alpha > 5/4$ can be due *only* to collimation of ejecta. The caveat of this criterion is that, as shown by Kumar & Panaitescu (2000), for collimated ejecta, the completion of most of $(\Delta\alpha)_j$ is spread over at least one decade in observer time for $s = 0$ and over at least two decades for $s = 2$. Therefore observations spanning a shorter time range will underestimate the true magnitude of the jet edge break, particularly in the case when the observer is not located close to the jet axis.

The results presented in §3.1 and §3.2 also lead to the following criteria for determining the location of ν_c relative to the optical and X -ray domains, and for identifying the type of external medium, from the optical and X -ray decay at the *same* time:

1. if $\alpha_o = \alpha_x$, then either ν_c is not between the optical and X -ray domains, or it is in this range but is quasi-constant in time. The latter may occur either in collimated ejecta during the sideways expansion phase, or before jet edge effects are important, in $s = 0$ models, if the inverse Compton cooling is the dominant process and if $p \simeq 8/3$ (see eq. [23]).
2. if $\alpha_x > \alpha_o$ (i.e. the X -ray decay is faster than in the optical), then $\nu_o < \nu_c < \nu_x$ and the external medium is homogeneous. Furthermore either the electron cooling is synchrotron dominated or, if Compton-dominated, $p < 8/3$.
3. if $\alpha_x < \alpha_o$, then $\nu_o < \nu_c < \nu_x$ and either the external medium is a wind-like or it is homogeneous and the electron cooling is inverse Compton-dominated ($Y > 1$), with $p > 8/3$.

Using the observed spectral slope in the optical range and the relative intensity of the X -ray and optical emission, one can eliminate some of the above cases, and further reduce the number of potentially good models for a given afterglow.

4. INDIVIDUAL AFTERGLOWS

The modeling of GRB afterglow light-curves is carried out by solving numerically equations (1), (2), (3), and (5), to determine the dynamics of the afterglow, and equation (19) to calculate the observed flux. The six unknown parameters \mathcal{E}_0 , θ_0 , n , p , ε_e , and ε_B are determined by minimizing the χ^2 between observed and model fluxes at the frequencies where most of the data is available. The jet initial Lorentz factor Γ_0 does not affect the afterglow emission if its evolution is quasi-adiabatic, because it drops out from the calculation of the jet Lorentz factor Γ as a function of observer time. When radiative losses are taken into account, Γ_0 may have an effect on the afterglow emission, as the magnitude of these losses depends on Γ_0 . However, the effect is weak and cannot be used to set significant constraints on Γ_0 . For simplicity, we keep a fixed $\Gamma_0 = 500$ in all numerical calculations.

In this work we restrict our attention to four afterglows for which radio, optical, X -ray light-curves and redshifts are available: GRB 980703, GRB 990123, GRB 990510, and GRB 991216, leaving out GRB 970508, whose optical light-curve cannot be entirely explained within the framework of our model, as it exhibited a brightening after 1 day, indicating a possible delayed energy injection, or fluctuations of the energy release parameters ε_e , ε_B or of the external density n .

The near-infrared (NIR) and optical magnitudes are converted to fluxes using the characteristics of photometric bands published by Campins, Rieke, & Lebofsky (1985), and Fukugita, Shimasaku & Ichikawa (1995). We assumed a 5% uncertainty in the magnitude–flux conversion. The NIR and optical fluxes are corrected for dust extinction using the interstellar reddening curves of Schild (1977), Cardelli, Clayton, & Mathis (1989), and Mathis (1990). A 10% uncertainty is assumed for the Galactic extinction.

4.1. GRB 980703

The emission of the afterglow of GRB 980703 is dominated by the host galaxy at only few days after the main event. No break has been detected in the optical within this time interval, which means that we can set only a lower limit on the jet opening angle, by requiring t_j to be sufficiently large.

The decay of the optical emission is characterized by a power-law index $\alpha_o = 1.17 \pm 0.25$ (Bloom et al. 1998), or $\alpha_o = 1.39 \pm 0.30$ (Castro-Tirado et al. 1999a), or $\alpha_o = 1.63 \pm 0.12$ (Vreeswijk et al. 1999), thus the average index is $\overline{\alpha_o} = 1.53 \pm 0.10$. The slope of the optical spectrum is $\beta_o = 2.71 \pm 0.12$ (Vreeswijk et al. 1999) at $t = 1.2$ day, and an X -ray decay index $\alpha_x = 1.33 \pm 0.25$ was found by Galama et al. (1998). Thus the observations give $\alpha_x - \overline{\alpha_o} = -0.20 \pm 0.27$. In view of the analytical considerations given in §3.1, the above $\alpha_x - \overline{\alpha_o}$ marginally rules out only a model with $s = 0$ and $\nu_c < \nu_x$.

For $s = 0$ and $\nu_o < \nu_c$, the optical decay index is $\alpha_o = (3p - 3)/4$, thus observations require that $p = 3.15 \pm 0.16$, which implies $\beta_o = (p - 1)/2 = 1.07 \pm 0.08$. Such a spectrum is much harder than observed, therefore consistency between observations and the fireball model can be achieved only if there is a substantial extinction. Given that the Galactic extinction toward this afterglow is $E(B - V) = 0.061$ (Bloom et al. 1998), it follows that most this extinction is due to the host galaxy. Vreeswijk et al. (1999) have shown that the synchrotron power-law spectrum becomes consistent with the observed one for an intrinsic extinction of $A_V = 1.45 \pm 0.13$. At the same

time the dereddened optical fluxes lead to $\beta_{ox} = 1.06 \pm 0.04$, which is consistent with the dereddened $\beta_o = (p - 1)/2$, implying that the cooling break is above X -rays.

For $s = 2$ and assuming $\nu_o < \nu_c < \nu_x$, leads to $\alpha_o = (3p - 1)/4$, therefore the observed α_o requires $p = 2.48 \pm 0.16$ and $\beta_o = (p - 1)/2 = 0.74 \pm 0.08$, which is again much harder than observed. Using the approximations found by Cardelli, Clayton, & Mathis (1989) for the UV interstellar reddening, one can show that dust extinction in the host galaxy steepens the synchrotron spectrum by $\Delta\beta_o \simeq 1.13A_V$ at the frequency which is red-shifted in the observer V -band. Therefore the synchrotron and observed spectra are consistent if $A_V = 1.74 \pm 0.13$, which is larger than for the $s = 0$ model because a wind-like medium yields softer spectra for the same decay index α . The corresponding dereddened optical emission has $\beta_{ox} = 1.11 \pm 0.04$, which falls between the limiting values, $(p - 1)/2$ and $p/2$, allowed by the synchrotron model.

Thus the afterglow of GRB 980703 may be explained by models with homogeneous external media, $\nu_o < \nu_x < \nu_c$, $p \sim 3.1$, and an intrinsic extinction $A_V = 1.45 \pm 0.13$, or by wind models with $\nu_o < \nu_c < \nu_x$, $p \sim 2.5$, and $A_V = 1.74 \pm 0.13$. Figure 1 shows an $s = 0$ model yielding an acceptable fit to the data.

4.2. GRB 990123

After the subtraction of the host galaxy, the r -band light-curve of the afterglow of GRB 990123 had a break around $t_b = 2$ day (Kulkarni et al. 1999a), with the asymptotic logarithmic slope changing by $\Delta\alpha_o \simeq 0.55 \pm 0.07$ from that at early times, $\alpha_{o,1} = 1.10 \pm 0.03$, to $\alpha_{o,2} = 1.65 \pm 0.06$ after t_b . The same break magnitude is implied by the power-law indices found by Castro-Tirado et al. (1999b). The reported slopes of the optical spectrum are $\beta_o = 0.75 \pm 0.23$ at $t = 1.2$ day (Galama et al. 1999), and $\beta_o = 0.8 \pm 0.1$ at $t = 1$ day (Kulkarni et al. 1999a). The optical-to- X -ray spectral slope β_{ox} reported by Galama et al. (1999) is $\beta_{ox} = 0.67 \pm 0.02$ at $t = 1.2$ day. Therefore $\beta_{ox} - \beta_o = -0.1 \pm 0.1$, indicating that the cooling break is not between optical and X -ray frequencies at $t \lesssim t_b$. The first BeppoSAX measurement (Heise et al. 1999) and the ASCA data (Murakami et al. 1999) give an X -ray decay index $\alpha_x = 1.17 \pm 0.10$ for $0.2 \text{ d} < t < 2 \text{ d}$, therefore $\alpha_x \simeq \alpha_{o,1}$, consistent with both $\nu_c < \nu_o$ and $\nu_x < \nu_c$.

If the break in the optical emission were due to the passage of the ν_c , then $\Delta\alpha_o > 1/4$ requires $s = 2$ and an increasing ν_c (see §3.1). Equation (26) and the observed $\Delta\alpha_o$ give $p = 2.46 \pm 0.08$. Then at $t < t_b$, when $\nu_c < \nu_o$, the optical-to- X -ray slope should be $\beta_{ox} = p/2 = 1.23 \pm 0.04$, clearly inconsistent with the observations. This shows that the optical break seen in this afterglow is not caused by the passage of ν_c .

A cooling frequency below optical cannot be accommodated by a jet model either, as the observed β_{ox} would imply $p = 2\beta_{ox} = 1.34 \pm 0.04$, leading to a decay index $\alpha_{o,1} = (3p - 2)/4 = 0.51 \pm 0.03$ (irrespective of the type of external medium) inconsistent with the observed value. Therefore the cooling frequency must be above X -ray, implying $p = 2\beta_{ox} + 1 = 2.34 \pm 0.04$. Then $s = 0$ leads to $\alpha_{o,1} = (3p - 3)/4 = 1.00 \pm 0.03$, while $s = 2$ yields $\alpha_{o,1} = (3p - 1)/4 = 1.50 \pm 0.03$. The latter case is clearly inconsistent with the observations.

From this analysis one can conclude that a successful model for the afterglow of GRB 990123 is that of a jet interacting with a homogeneous external medium, with parameters such that $\nu_o < \nu_x < \nu_c$ at $t < t_b$, and $p \sim 2.3$. This value of p im-

plies an optical decay index $\alpha_{o,2} \sim p$ substantially larger than found by Kulkarni et al. (1999a). However, the observations made after $t_j \sim 2$ day do not span a sufficiently long time and may underestimate the asymptotic $\alpha_{o,2}$.

The radio and optical data at $t = 1.2$ day give a radio-to-optical slope $\beta_{ro} = 0.27 \pm 0.04$. If the injection break were below radio frequencies (ν_r) at this time, then $p = 2\beta_{ro} + 1 = 1.54 \pm 0.08$, inconsistent with the value derived above from the optical and X -ray data. Therefore $\nu_r < \nu_i$ at $t < t_j$. But in this case, as pointed out by Kulkarni et al. (1999a), the radio emission should rise until ν_i falls below ν_r . For a jet, this rise stops around t_j and is followed by a constant emission until $\nu_i = \nu_r$, after which the radio flux should decrease. However, the radio emission of 990123 exhibits a strong dimming around 2 days (see Figure 2) which, as suggested by the argument above, cannot be explained by the forward shock emission in a jet model (see the radio light-curve shown in Figure 2 with dashed line). We shall assume that the two earliest radio fluxes are produced by another radiation mechanism, for instance emission by cooled electrons that were accelerated by the reverse shock (Sari & Piran 1999) or emission from less relativistic ejecta surrounding the jet, and use these fluxes only as upper limits for the forward shock emission.

Figure 2 shows a jet model for the emission of 990123. The K -band fluxes observed after 10 days lie above the model prediction, being inconsistent with an achromatic break resulting from collimation of ejecta. If the optical flash of GRB 990123 was due to a reverse shock propagating in the ejecta (Sari & Piran 1999), and if the peak of this flash, seen at $t \sim 50$ seconds, corresponds to the fireball deceleration timescale, then the isotropic equivalent energy and external density of the model in Figure 2 imply that the fireball initial Lorentz factor was $\Gamma_0 = 1400 \pm 700$. Alternatively, the optical flash may have been caused by internal shocks in an unstable wind (Mészáros & Rees 1999, Kumar & Piran 2000), in which case Γ_0 is more uncertain.

4.3. GRB 990510

The optical afterglow of GRB 990510 exhibited a break around $t_b = 1.5$ day, whose reported magnitude is $\Delta\alpha_o = 1.80 \pm 0.20$ (Israel et al. 1999) in the V -band, $\Delta\alpha_o = 1.67 \pm 0.02$ (Stanek et al. 1999), to $\Delta\alpha_o = 1.36 \pm 0.05$ (Harrison et al. 1999). The optical asymptotic decay indices found by Harrison et al. (1999) are $\alpha_{o,1} = 0.82 \pm 0.02$ and $\alpha_{o,2} = 2.18 \pm 0.05$. The X -ray decay index was $\alpha_x = 1.42 \pm 0.07$ (Kuulkers et al. 1999) at $0.3 \text{ d} < t < 2 \text{ d}$, while the optical spectral slope was $\beta_o = 0.61 \pm 0.12$ (Stanek et al. 1999) at $t = 0.9$ day. The available data imply an optical-to- X -ray slope $\beta_{ox} = 0.90 \pm 0.04$ at $t = 0.72$ day.

Even the smallest reported $\Delta\alpha_o$ is above $5/4$, therefore the break seen in the optical emission cannot be due to the passage of ν_c (see §3.3) and must have been caused by jet effects. From $\beta_{ox} - \beta_o = 0.29 \pm 0.13$ one can infer that ν_c is between optical and X -rays. The same conclusion is suggested by $\alpha_{o,1} < \alpha_x$, however the X -ray observations were made at times close to t_j , thus the observed X -ray decay index may overestimate the asymptotic α_x at earlier times.

For a homogeneous medium $\alpha_{o,1} = (3p - 3)/4$, therefore observations require that $p = 2.09 \pm 0.03$, thus the analytically expected values of $\alpha_{o,2} \sim p$ and $\beta_o = (p - 1)/2 = 0.55 \pm 0.02$ are consistent with those observed. For a wind-like medium $\alpha_{o,1} = (3p - 1)/4$, requiring that $p = 1.43 \pm 0.03$, which leads to an optical slope $\beta_o = (p - 1)/2 = 0.22 \pm 0.02$ inconsis-

tent even with the softest optical spectrum reported by Stanek et al. (1999): $\beta_o = 0.46 \pm 0.08$. Such a small value of p also implies $\beta_{ox} \leq p/2 = 0.72 \pm 0.02$, again inconsistent with the observations. Thus a wind-like medium is ruled out.

Therefore the afterglow of GRB 990510 can be accommodated by a model with $s = 0$, $\nu_o < \nu_c < \nu_x$ and $p \sim 2.1$. Note that the model shown in Figure 3 fits well the X -ray data, the light-curve steepening being very slow.

4.4. GRB 991216

The optical decay index of the afterglow of GRB 991216 was $\alpha_{o,1} = 1.22 \pm 0.04$ (Halpern et al. 2000, Sagar et al. 2000) at $t < t_b = 2$ day. Halpern et al. have shown that a broken power-law optical light-curve with $\alpha_{o,2} = 1.53 \pm 0.05$ at $t > t_b$ plus the contribution $R = 24.8 \pm 0.1$ from a galaxy located at ~ 1 arcsecond from the optical transient explains well the observations. Sagar et al. (2000) find that two measurements made after t_b are dimmer by 2σ than the power-law extrapolation from earlier fluxes. Therefore there is evidence that the decay of the optical emission of the 991216 afterglow steepened by $\Delta\alpha_o = 0.31 \pm 0.06$.

The X -ray data span 1.3 decades in time before t_b and have $\alpha_x = 1.62 \pm 0.07$ (Frail et al. 2000, Halpern et al. 2000), leading to $\alpha_x - \alpha_{o,1} = 0.40 \pm 0.08$. The optical spectrum is puzzling, exhibiting a turn-over at the J -band at $t \simeq 1.5$ day (Frail et al. 2000, Halpern et al. 2000), although the J and K -band measurements reported by Garnavich et al. (2000) restore a power-law spectrum of slope $\beta_o = 0.58 \pm 0.08$ at $t = 1.7$ day. Garnavich et al. (2000) have pointed out that, if extinction is overestimated by a factor 1.3–1.5 close to the Galactic plane (Stanek et al. 1999), the dereddened optical spectrum could be softer: $\beta_o = 0.87 \pm 0.08$. The optical-to- X -ray spectral slope is $\beta_{ox} = 0.80 \pm 0.10$ (Garnavich et al. 2000, Halpern et al. 2000) at $t = 1.7$ day.

The faster decay seen in the X -rays than in the optical before t_b requires $\nu_o < \nu_c < \nu_x$ and a homogeneous external medium (see §3.3), in which case it is expected that $\alpha_x - \alpha_{o,1} \leq 1/4$. This difference is 2σ below the observed value. For $\nu_o < \nu_c$, the analytical optical decay index is $\alpha_{o,1} = (3p - 3)/4$, thus observations imply $p = 2.63 \pm 0.05$. This leads to $\beta_o = (p - 1)/2 = 0.82 \pm 0.03$, which is consistent with the softer dereddened suggested by Garnavich et al. (2000). However, for such a spectrum, $\beta_{ox} - \beta_o = -0.07 \pm 0.13$ does not support a cooling frequency between optical and X -rays.

If the optical light-curve break were due to the passage of ν_c then $\Delta\alpha_o = 1/4$, consistent with the observations. Then at $t \sim t_b$, when $\nu_c \sim \nu_o$, the optical-to- X -ray slope should be $\beta_{ox} = p/2 = 1.32 \pm 0.03$, clearly inconsistent with the observations. Therefore the break in the optical emission of 991216 was not caused by the passage of ν_c . Instead, the small magnitude optical break could be explained by jet effects if the short time baseline of the observations after t_j capture only a part of the full steepening.

However there are some major difficulties that a jet model with $\nu_o < \nu_c < \nu_x$ encounters. The decay index of the radio emission $\alpha_r = 0.82 \pm 0.02$ (Frail et al. 2000) at $t \gtrsim 1$ day requires the injection break ν_i to be below 10 GHz, which leads to a radio-to-optical spectral slope $\beta_{ro} = \beta_o = 0.6 \div 0.9$, while observations give $\beta_{ro} = 0.20 \pm 0.05$ at 2 days. Furthermore, the decay indices at radio and optical frequencies should be the same, yet observations show that $\alpha_{o,1} - \alpha_r = 0.40 \pm 0.04$. The discrepancy is large enough to suggest that a model with the above features cannot accommodate the optical and all the

radio data. A possible solution is to “decouple” α_γ and $\alpha_{o,1}$ by assuming that the radio emission until several days has a different origin, as we assumed for the early radio emission of 990123. Then the quasi-flat behavior of the radio data at 8–50 days (Figure 4) is suggestive of a jet undergoing lateral spreading and with ν_i above radio until 50 days, as this is the only way of obtaining a constant flux if the external medium is homogeneous (the analytical prediction for $\nu < \nu_i$ and after the jet edge is seen, $F_\nu \propto t^{-1/3}$, is based on some approximations that are not sufficiently accurate; numerically we obtain a slightly different behavior $F_\nu \sim const$).

There is, however, a model which does not require another emission mechanism besides the forward shock or a two-component structure of the jet (Frail et al. 2000), and which can accommodate the entire radio data. The almost constant flux exhibited by the radio emission at 1–3 days (Figure 4) can be explained by jet expanding laterally before 1 day, with the steepening of the radio emission at several days being due to the ν_i -passage. Then the steepening of the optical decay at few days is not due to jet effects, as suggested by Halpern et al. (2000), but to the passage of a spectral break. The cooling frequency ν_c does not offer a self-consistent picture: it should be above optical shortly before 2 days, as required by $\alpha_x > \alpha_{o,1}$ and, according to equation (28), it should increase in time because during the jet sideways expansion phase, thus it cannot cross the optical domain.

Within our afterglow modeling there is only one remaining possibility: the steepening of the optical emission is due to the passage of the ν_M frequency associated with the high energy break of the electron distribution (eq. [10]). As the jet model yields $F_\nu \propto t^{-p}$ at all frequencies above ν_i (eq. [29]), the observed $\alpha_{o,1}$ implies a very hard electron distribution with $p \sim 1.2$. Then the observed $\beta_o = 0.58 \pm 0.08$ requires $\nu_c < \nu_o$ at 2 days, to obtain consistency with the analytical expectation $\beta_o = p/2 \sim 0.6$.

Such a jet model with a hard electron distribution and cooling frequency below optical is shown in Figure 4. The observed optical emission steepens only mildly after 2 days, therefore the high energy break at γ_M is not too strong. For simplicity we have approximated this break as a softening of the electron distribution from γ^{-p} to $\gamma^{-(p+\delta p)}$ at γ_M , with δp a free parameter. The location of ν_m is set by the fractional electron energy $\epsilon = 0.5$ up to γ_M (eq. [10]). Smaller values of ϵ , but larger than 0.1, also provide acceptable fits. The afterglow shown in Figure 1 is mildly relativistic after 10 days, so that departures from the analytically expected light-curve $F_{\nu > \nu_i} \propto t^{-p}$ allow the model to accommodate both the $t^{-1.2}$ optical decay before 2 days and the $t^{-0.8}$ fall-off of the radio emission after 10 days. As illustrated in Figure 4 the effect of interstellar scintillation (Goodman 1997) is essential in explaining the departures between the observations and the model radio fluxes.

We note that a jet interacting with a wind-like external medium with $A_* \sim 1$ yields fits with acceptable χ^2 , but produces millimeter fluxes that exceed the 2σ upper limits shown in Figure 4 (right panel).

4.5. Parameter Ranges and Afterglow Energetics

The electron index p and the initial jet opening angle θ_0 are determined by the index of the power-law emission decay and by the time when jet effects set in, respectively (see eqs. [27], [21], and [22]). The remaining four model parameters, E_0 , n , ϵ_e , and ϵ_B , can be determined from the three break frequencies ν_a , ν_i , ν_c (see eqs. [8], [13], [16], and [17]), and the syn-

chrotron flux at the peak of the spectrum. Finding the location of the spectral breaks requires observations spanning a wide frequency range, from below the lowest break (self-absorption) to above the highest break (cooling, more likely). Even if this requirement is satisfied, observations in only three domains (radio, near infrared–optical, and X -ray) do not determine all the spectral breaks unless the unconstrained break(s) cross(es) an observing frequency. This does not seem to be the case for the afterglows analyzed here, observations providing at most three “strong” constraints for four free model parameters. The number of constraints is even smaller if the interval between two adjacent observational frequencies does not contain a spectral break. For instance, in the case where $\nu_x < \nu_c$, the X -ray fluxes can be predicted from the optical emission and the spectral slope $\beta(p)$. If consistency is found between the model and the observed X -ray fluxes, i.e. if the condition $\nu_x < \nu_c$ is indeed satisfied, then the X -ray data will provide only a “weak” constraint, as they set only a lower bound on the cooling break frequency.

Therefore the uncertainty in the parameters of the afterglows analyzed in this work arises from that the number of effective observational constraints is smaller than the number of model parameters. To assess these uncertainties, we find sets of parameters which yield acceptable fits to the data, for a given isotropic equivalent energy \mathcal{E}_0 . The distributions of the parameters for which the probability of exceeding the χ^2 of the data is at least 20% are shown in Figures 5 and 6. Note that θ_0 ranges from about 1° to 4° and that the external medium density spans four decades. Figure 6 shows the lack of a pattern in the electron and magnetic field parameters among the four afterglows. As expected, the index p is well constrained for each afterglow, the light-curve decay being very sensitive to it. Note that, for the afterglows modeled here, p does not have a universal value.

Figure 7 shows the distributions of jet energy $E_0 = (\mathcal{E}_0/2)(1 - \cos \theta_0)$ and of the burst γ -ray efficiency, defined as the ratio of the isotropic equivalent \mathcal{E}_γ of the energy released by the GRB in the 20 keV – 1 MeV range to the total fireball energy $\mathcal{E}_\gamma + \mathcal{E}_0$. The \mathcal{E}_γ was calculated from the reported fluences Φ_γ above 20 keV (Kippen et al. 1998-9) and the measured redshifts: $\mathcal{E}_\gamma \sim 10^{53}$ erg for GRB 980703, $\mathcal{E}_\gamma \sim 3 \times 10^{54}$ erg for GRB 990123, $\mathcal{E}_\gamma \sim 2 \times 10^{53}$ erg for GRB 990510, and $\mathcal{E}_\gamma \sim 7 \times 10^{53}$ erg for GRB 991216. Note that, when θ_0 can be determined from observations, the jet energies are clustered in the 10^{50} to 10^{51} erg range, and that the minimum efficiency for GRBs 990123 and 991216 exceeds 20%.

5. CONCLUSIONS

We model the emission of GRB afterglows in the framework of collimated, uniform, lateral spreading jets interacting with an external medium. The model was used to determine the initial jet energy E_0 , opening angle θ_0 , external medium density n , and parameters ϵ_e and ϵ_B quantizing the minimum random Lorentz factor of shock-accelerated electrons and the strength of the magnetic field, respectively, for the afterglows of GRB 980703, 990123, 990510, and 991216.

As illustrated in Figures 5 and 6, the jet aperture θ_0 and the index p of the power-law distribution of electrons injected in the down-stream region are well constrained by observations, as the effects of collimation are seen at a time which depends strongly on θ_0 (eq. [27]), while p determines the afterglow decay rate (eqs. [21], [22], [29]). Other model parameters – E_0 , n , and ϵ_B – are less well determined as observations in three frequency

domains (radio, optical, and X -ray) provide at most three constraints. Observations in a fourth domain, sub-millimeter, millimeter, or far-infrared, could help determine all the afterglow parameters, provided that the spectral breaks are located between adjacent observational frequencies.

Analysis of the available data for the 990123 and 990510 afterglows and the jet interpretation of the break exhibited by their optical emissions rule out a wind-like profile for the medium which decelerates the jet. However, the emission of the 980703 and 991216 afterglows can be accommodated by both types of external media (homogeneous or a pre-ejected wind). For 980703, 990123, and 990510, the allowed range of external densities is below 1 cm^{-3} , indicating that these bursts did not occur in hydrogen clouds.

For those afterglows with optical light-curve breaks we find jet energies lying mostly in the 10^{50} – 10^{51} erg range (Figure 7), and jet initial half-angles below 4° . For the afterglow of GRB 970508, the only one observed in radio, optical and X -ray that is not included in this work due to its non-standard optical and X -ray brightening, Frail, Waxman & Kulkarni (2000) found a

similar jet energy, $E_0 = 5 \times 10^{50}$ erg, a much larger initial half-angle, $\theta_0 \sim 30^\circ$, and an external density $n \sim 1 \text{ cm}^{-3}$.

The minimum BATSE range (20 keV – 1 MeV) efficiency of the afterglows whose optical behavior indicates that the ejecta was well collimated ranges from 3% to 30% (Figure 7). The former limit is within the reach of current calculations of internal shock efficiency (Kumar 1999, Lazzati et al. 1999, Panaitescu, Spada & Mészáros 1999), but the latter exceeds it. However, if the energy distribution within the jet aperture is far from isotropy, such that the GRBs we see have an energy-per-solid angle peaking in the direction toward the observer, then the minimum required efficiency can be significantly smaller.

A.P. acknowledges support from the Lyman Spitzer Jr. fellowship. The work of P.K. is supported in part by NSF grant phy-0070928. The authors commend the work of Jochen Greiner, who maintains a very useful compilation of the available information on GRB afterglows at <http://www.aip.de:8080/~jcg/grbgen.html>.

REFERENCES

- Beloborodov, A. 2000, ApJ, 539, L25
 Beuermann, K. et al. 1999, A&A, 352, L26
 Bloom, J. et al. 1998, ApJ, 508, L21
 Bloom, J. et al. 2000, GCN* 756
 Campins, H., Rieke, G., & Lebofsky, M. 1985, AJ, 90, no 5, 896
 Cardelli, J., Clayton, G., & Mathis, A. 1989, ApJ, 345, 245
 Castro-Tirado, A. et al. 1999a, ApJ, 511, L85
 Castro-Tirado, A. et al. 1999b, Science, 283, 2069
 Corbet, R. et al. 1999, GCN* 506
 Djorgovski, S. et al. 1998, ApJ, 508, L17
 Djorgovski, S. et al. 1999, GCN* 510
 Frail, D. et al. 1999, GCN* 141
 Frail, D., Waxman, E., & Kulkarni, S. 2000, ApJ, 537, 191
 Frail, D. et al. 2000, ApJ, 538, L129
 Fruchter, A. et al. 1999, GCN* 386
 Fruchter, A. et al. 2000, GCN* 757
 Fukugita, M., Shimasaku, K., & Ichikawa, T. 1995, PASP, 107, 945
 Galama, T. et al. 1998, GCN* 145
 Galama, T. et al. 1999, Nature, 398, 394
 Garnavich, P. et al. 2000, ApJ, 543, 61
 Goodman, J. 1997, New Astronomy, 2, 49
 Halpern, J. et al. 2000, ApJ, 543, 697
 Harrison, F. et al. 1999, ApJ, 523, L121
 Heise, J. et al. 1999, IAU 7099, GCN* 202
 Huang, Y., Gou, L., Dai, Z., & Lu, T. 2000, ApJ, 543, 90
 Israel, G. et al. 1999, A&A, 348, L51
 Kelson, D. et al. 1999, IAU 7096
 Kippen, R. et al. 1998-9, GCN* 143, 224, 322, 504
 Kulkarni, S. et al. 1999a, Nature, 398, 389
 Kulkarni, S. et al. 1999b, ApJ, 522, L97
 Kumar, P. 1999, ApJ, 523, L113
 Kumar, P. & Piran, T. 2000, ApJ, 532, 286
 Kumar, P. & Panaitescu, A. 2000, ApJ, 541, L9
 Kuulkers, E. et al. 2000, ApJ, 538, 638
 Lazzati, D., Ghisellini, G., & Celotti, A., 1999, MNRAS 309, L13
 Mathis, J. 1990, ARA&A, 28, 37
 Mészáros, P. & Rees, M.J. 1994, ApJ, 430, L93
 Mészáros, P. & Rees, M.J. 1999, MNRAS, 306, L39
 Murakami, T. et al. 1999, GCN* 228
 Odewahn, S. et al. 1999, GCN* 261
 Panaitescu, A., Mészáros, P., & Rees, M.J. 1998, ApJ, 503, 314
 Panaitescu, A., Spada, M., & Mészáros, P. 1999, ApJ 522, L105
 Panaitescu, A. & Kumar, P. 2000, ApJ, 543, 66
 Pietrzynski, G. & Udalski, A. 1999, GCN* 319, 328
 Piro, L. 1999, GCN* 500
 Rhoads, J. 1999, ApJ, 525, 737
 Rol, E. et al. 1999, GCN* 491
 Sagar, R., Mohan, V., Pandey, A., & Castro-Tirado, A. 2000, BASI, 28, 15
 Sari, R., Piran, T., & Narayan, R. 1998, ApJ, 497, L17
 Sari, R. & Piran, T. 1999, ApJ, 517, L112
 Schaefer, B. 2000, GCN* 517
 Schild, R. 1977, AJ, 82, 337
 Stanek, K., Garnavich, P., Kaluzny, J., Pych, W., & Thompson, I. 1999, ApJ, 522, L39
 Takeshima, T. 1999, GCN* 478
 Vreeswijk, P. et al. 1999, ApJ, 523, 171
 Vreeswijk, P. et al. 2000, GCN* 751
 Walker, M. 1998, MNRAS, 294, 307
 * GCN Circulars can be found at <http://gcn.gsfc.nasa.gov/gcn/>

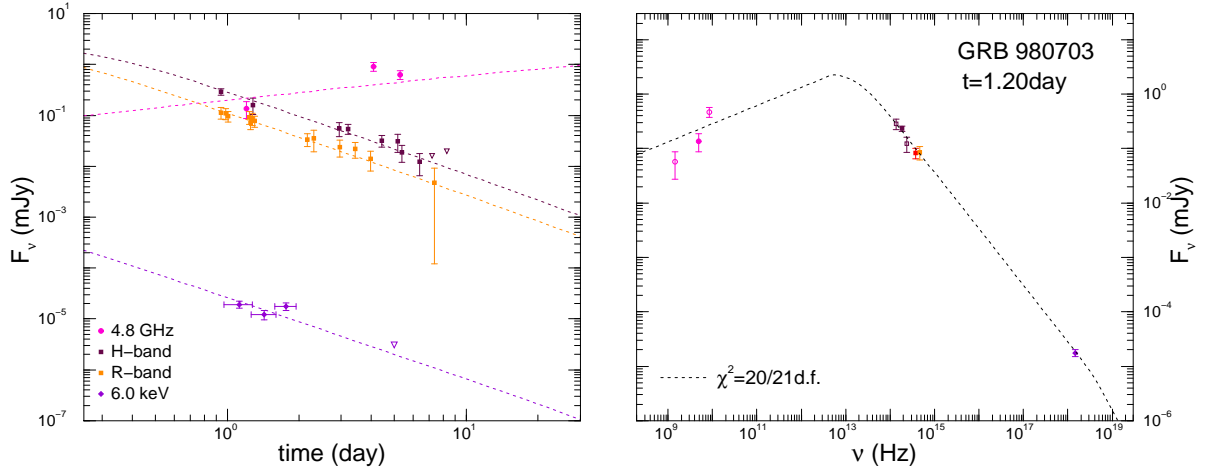


FIG. 1.— Light-curves (left panel) and $t = 1.20$ day spectrum (right panel) for the afterglow of GRB 980703 ($z = 0.966$). Radio data are from Frail et al. (1999). We assume 20–40% uncertainty when no errors were reported, the larger errors being for earlier or lower frequency observations, the smaller for later or higher frequencies. Optical fluxes are calculated from the magnitudes published by Bloom et al. (1998), Castro-Tirado et al. (1999a), and Vreeswijk et al. (1999). The host galaxy contribution (Vreeswijk et al. 1999) is subtracted. Optical fluxes are corrected for a Galactic extinction of $E(B - V) = 0.061$ (Bloom et al. 1998) and for the host galaxy extinction inferred by Vreeswijk et al. (1999): $A_V = 1.45 \pm 0.13$. X-ray fluxes are calculated from the 2–10 keV band fluxes reported by Vreeswijk et al. (1999). Triangles indicate 2σ upper limits. Right panel: optical measurements closest to $t = 1.20$ day are extrapolated to this time using $F_\nu \propto t^{-\alpha}$, with the indices α reported by Vreeswijk et al. (1999). Open symbols for radio fluxes are extrapolations from the 4.1 and 5.3 days measurements of Frail et al. (1999) with the analytically expected behavior $F_\nu \propto t^{1/2}$. The model shown has $\chi^2 = 20$ for 21 df and the following parameters: $\mathcal{E}_0 = 2.9 \times 10^{54}$ erg (isotropic equivalent energy), $n = 7.8 \times 10^{-4} \text{ cm}^{-3}$, $\varepsilon_e = 0.075$, $\varepsilon_B = 4.6 \times 10^{-4}$, $p = 3.08$. The initial jet angle is lower bounded by the condition that no effects of collimation are seen until the later available data, which leads to $\theta_0 \gtrsim 2.7^\circ$. Radiative losses amount to 1.6% at 10 days. Synchrotron emission is the main electron radiative cooling mechanism at all times shown here.

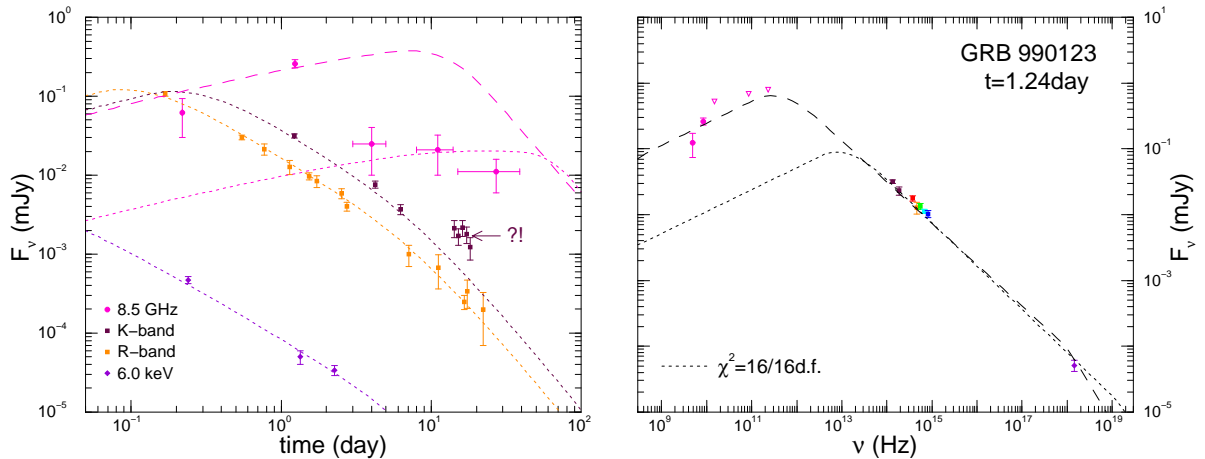


FIG. 2.— Light-curves and $t = 1.24$ day spectrum for the afterglow of GRB 990123 ($z = 1.61$). Radio data are from Kulkarni et al. (1999b). Optical fluxes are calculated from the magnitudes reported by Kulkarni et al. (1999a) by subtracting the host galaxy contribution $F_r = 0.5 \pm 0.1 \mu\text{Jy}$ and $K = 22.1 \pm 0.3$, and from the HST measurement reported by Odewahn et al. (1999). Fluxes are corrected for a Galactic extinction of $A_r = 0.04$ (Kulkarni et al. 1999a). X-ray fluxes are calculated from the 2–10 keV fluxes reported by Heise et al. (1999) and Murakami et al. (1999), using the quoted spectral indices and assuming a 10% error. Other data, used for the spectrum shown in the right panel, are from Galama et al. (1999) and Castro-Tirado et al. (1999b), and are extrapolated to $t = 1.24$ day using the optical decay indices given in Castro-Tirado et al. (1999b). Triangles indicate 2σ upper limits. The model shown has $\chi^2 = 16$ for 16 df, excluding the first two radio measurements and the group of late K-band observations (which would increase χ^2 by $\Delta\chi^2 = 36$ for), and parameters: $E_0 = 4.6 \times 10^{50}$ erg (initial jet energy), $\theta_0 = 2.0^\circ$, $n = 4.7 \times 10^{-4} \text{ cm}^{-3}$, $\varepsilon_e = 0.13$, $\varepsilon_B = 1.3 \times 10^{-4}$, $p = 2.32$. The steepening of the optical decay is due to jet effects. About 9% of the afterglow energy is radiated until 30 days. Inverse Compton scatterings dominate the electron radiative cooling until several days. The model shown with *dashed* line yields a good fit to the optical and X-ray data, but matches only the first two radio measurements, over-predicting the late time radio emission.

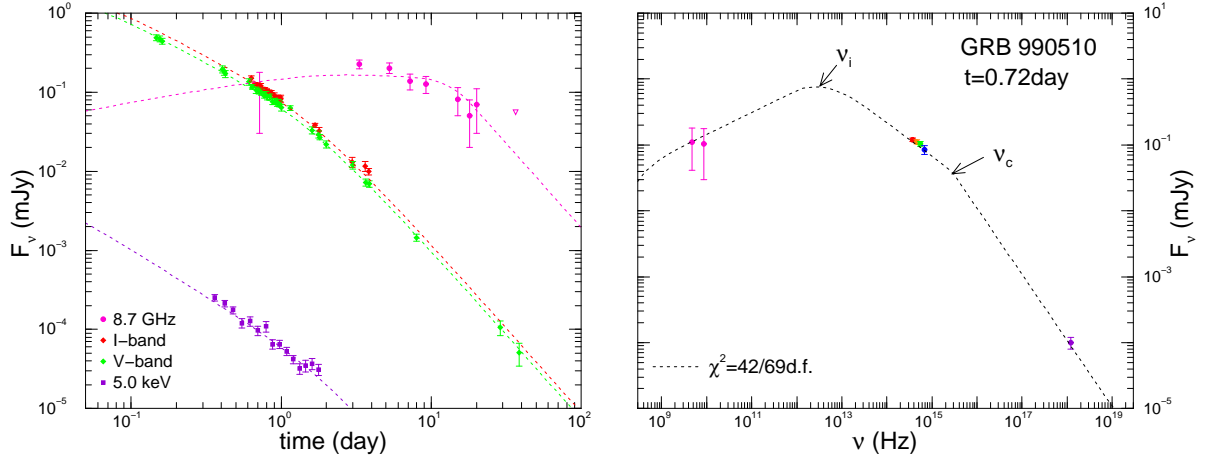


FIG. 3.— Light-curves and $t = 0.72$ day spectrum for the afterglow of GRB 990510 ($z = 1.62$). Radio data are from Harrison et al. (1999). The triangle indicates a 2σ upper limit. Optical fluxes are obtained from the magnitudes reported by Beuermann et al. (1999), Fruchter et al. (1999), Harrison et al. (1999), Israel et al. (1999), Pietrzyński & Udalski (1999), and Stanek et al. (1999). These fluxes are corrected for dust extinction with $E(B - V) = 0.20$ (Harrison et al. 1999, Stanek et al. 1999). The uncertain, small contribution of the host galaxy, $V_g \gtrsim 28.0$ (Bloom et al. 2000, Fruchter et al. 2000), is ignored. X -ray fluxes are calculated from the 2–10 keV band fluxes and spectral slope published by Kuulkers et al. (2000). The model shown has $\chi^2 = 42$ for 69 df, and parameters: $E_0 = 3.0 \times 10^{50}$ erg, $\theta_0 = 2.7^\circ$, $n = 0.14 \text{ cm}^{-3}$, $\varepsilon_e = 0.046$, $\varepsilon_B = 8.6 \times 10^{-4}$, $p = 2.01$. The steepening of the optical decay is due to the collimation of ejecta. The radiative losses amount to 53% at 40 days. At all times shown here, inverse Compton scatterings is the dominant electron radiative cooling mechanism.

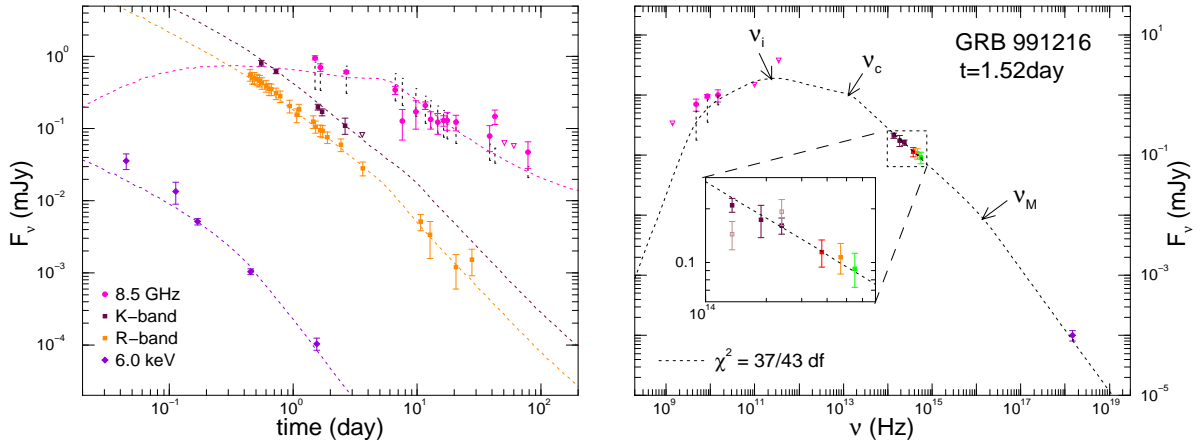


FIG. 4.— Light-curves and $t = 1.52$ day spectrum for the afterglow of GRB 991216 ($z = 1.02$). Radio data are from Rol et al. (1999) and Frail et al. (2000). Optical fluxes are calculated from the magnitudes published by Garnavich et al. (2000), Halpern et al. (2000), Sagar et al. (2000), and Schaefer (2000). We subtracted the contamination from a galaxy located near the OT, estimated by Halpern et al. (2000) at $R = 24.8 \pm 0.1$ (the host galaxy, identified by Vreeswijk et al. 2000, has $R = 26.9 \pm 0.4$). Optical fluxes are corrected for a Galactic extinction of $E(B - V) = 0.63$ (Garnavich et al. 2000, Halpern et al. 2000). X -ray fluxes are calculated from the 2–10 keV fluxes reported by Corbet et al. (1999), Piro et al. (1999), and Takeshima et al. (1999). Right panel: the measurements closest to $t = 1.52$ day are extrapolated to this time using the power-law scaling found by Garnavich et al. (2000) in the near-infrared and by Halpern et al. (2000) in the optical. Inset: J and K measurements of Halpern et al. (2000) are shown with open symbols, while those reported by Garnavich et al. (2000), consistent with a power-law spectrum, are indicated with filled symbols. Triangles indicate 2σ upper limits. The model shown has $\chi^2 = 37$ for 43 df and parameters $E_0 = 0.89 \times 10^{50}$ erg, $\theta_0 = 3.4^\circ$, $n = 1.6 \text{ cm}^{-3}$, $\varepsilon_e = 0.024$, $\varepsilon_B = 0.073$, $p = 1.36$, $\delta p = 0.7$. The ν_M frequency is set by the fractional electron energy, assumed $\epsilon = 0.5$. The steepening of the X -ray and optical fall-off is due to the passage of the ν_M break. Vertical dotted lines indicate the amplitude of the interstellar scintillation, which we model following the treatment given by Walker (1998). The afterglow radiates 82% of its energy until 80 days. The electrons cool radiatively mainly through synchrotron emission after few days.

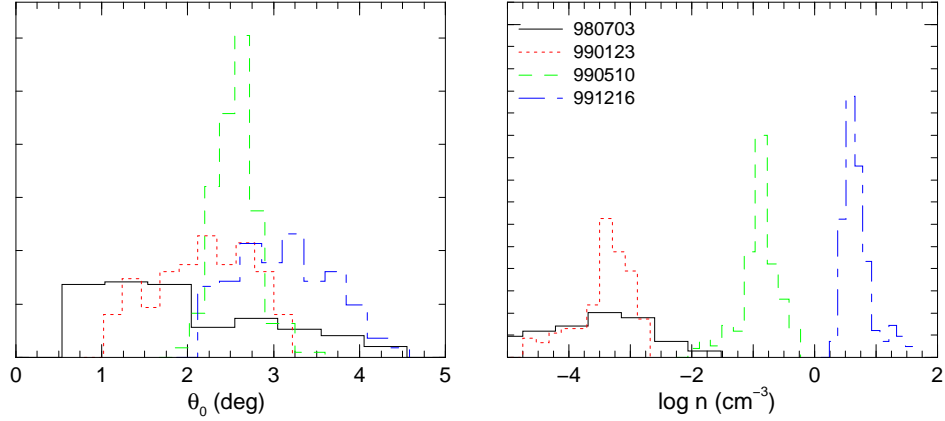


FIG. 5.— Distributions of the parameters θ_0 (jet initial opening) and n (external medium density) obtained from fits to the afterglows of GRB 980703, 990123, 990510, and 991216. For the models with these parameters the probability of exceeding the χ^2 of the data is at least 20%. The decay of the afterglow of GRB 980703 does not show evidence for collimation of ejecta until several days. The initial jet apertures shown in this case are obtained by requiring that $t_j = 5$ day (eq. [27]), therefore they are lower limits of the true θ_0 .

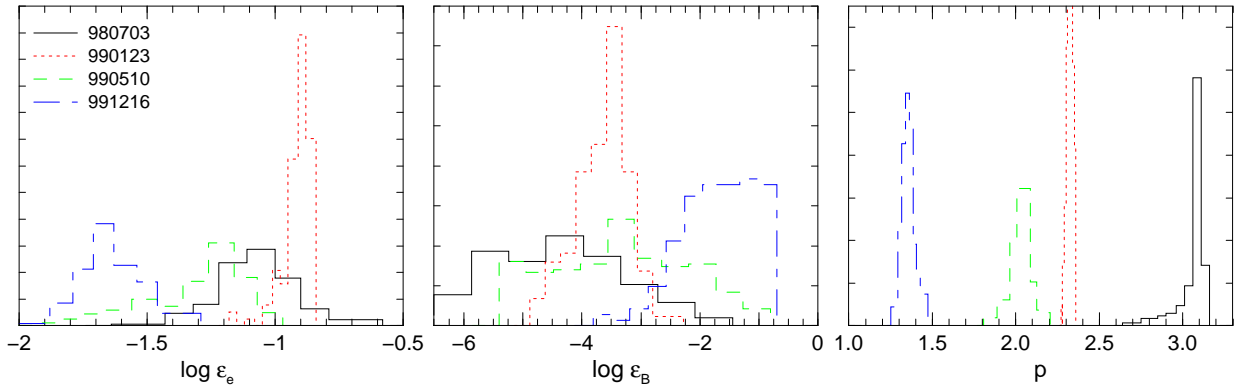


FIG. 6.— Distributions of the parameters ϵ_e (for the minimum energy of the injected electrons), ϵ_B (fractional energy in magnetic field), and p (exponent of the injected power-law distribution) for the same models as in Figure 5. Note that these four afterglows have distinct allowed ranges for p .

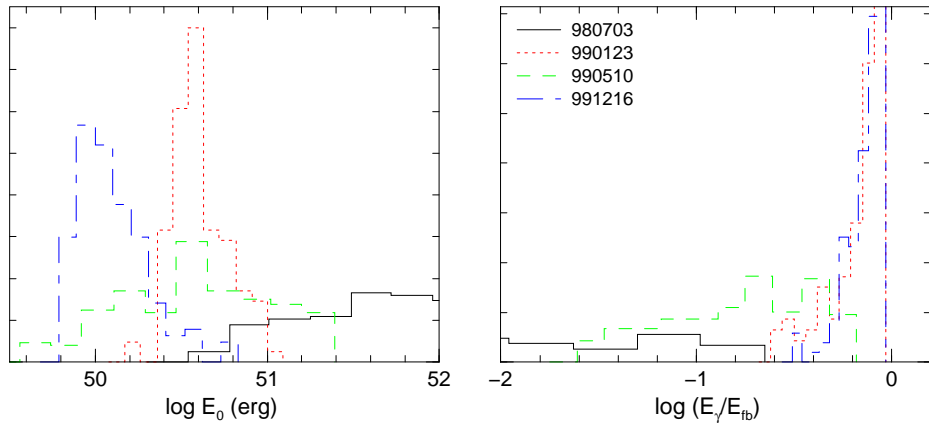


FIG. 7.— Distribution of the jet energy E_0 and GRB radiative efficiency for the models whose parameters are shown in Figures 5 and 6. The radiative efficiency is the ratio of the energy \mathcal{E}_γ released by the GRB in the BATSE range (approximately 20 keV – 1 MeV), assuming spherical symmetry, and the initial fireball energy $\mathcal{E}_{fb} = \mathcal{E}_\gamma + \mathcal{E}_0$, where \mathcal{E}_0 is the isotropic equivalent of the ejecta energy which yields acceptable fits to the afterglow emission. For GRB 980703 we used the lower limits on θ_0 shown in Figure 5 to calculate the jet energy.